Dedication

This research is dedicated to . . .

THE SOUL MY MOTHER….

MY FATHER...

….ALL MY FAMILLY

AND EVERY ONE WHO WISHED GOOD FOR ME

TO THE FACE OF GOD WHO HELP ME, ALL THROUGH THIS WORK,

AND EVER AFTER, WHOM I ASK MORE ASSISTANCE AND SUPPORT

ACKNOLODEGMENT

First and foremost, I would like to thank God for the grace of completing this work, also I would like to express my sincere gratitude to my advisor Dr. **Ahmed mostafa abokoona** for her guidance, stimulating suggestions, encouragement all the time, so it was a great pleasure to do this thesis under her supervision.

I am thankful to Dr. Ali Abdelrazig who provided me with the help which I required for the completion of this work. Finally, the biggest thanks to my family and in particular parents.

List of Figures

List of Table

List of Abbreviations

FDA	food and drug administration
BSE	breast self-examination
CC	craniocaudal position
MLO	mediolateral oblique position
FFDM	full-field digital mammography
FID	focus image distance
Mo	molybdenum
HVL	half-value layer
ACR	American College of Radiology
CFR	code of federal regulations
MQSA	mammography quality standards act
AEC	automatic exposure-control
CDF	contrast degradation factor
SPR	scatter-to-primary ratio

List of Contents

Abstract

Mammography continues to be the primary imaging tool in the detection of early breast cancer. Because of the overall increase in the use of medical ionizing radiation, many patients and their physicians are appropriately concerned about individual radiation dose and specifically concerned about the risks of radiation from mammography.

The aim of this study was to investigate scatter radiation intensity around modern digital mammography systems in three hospitals under clinical conditions. The readings were carried out using RADOS (RDS-120 Universal Survey Meter). Scatter radiation was measured at different distance in four areas around the mammography unit; these areas were the control room, Technician office, neighboring offices and Waiting area of mammography room. The distance from the mammogram and the four regions was measured. All measurements were taken in Craniocaudal projection.

The result of the study showed that the readings of scattered radiation were detected in control room (0.5μSv/h) and neighboring (0.2 μSv/h) office in hospital A. It was also detected in the neighboring office (0.9 μSv/h) in hospital B, while it was noticed in the waiting area (0.8 μSv/h) in hospital C.

These scatter measurements could be used in a shielding calculation and compared with current shielding design criteria to determine whether additional radiation protection or alteration to present shielding was required.

الخلاصة

التصوير الشعاعي للثدي هو أداة التصوير الأولية في الكشف عن سرطان الثدي المبكر. وبسبب الزيادة الإجمالية في استخدام الإشعاعات المؤينة الطبية، فإن العديد من المرضى وأطباءهم يشعرون بالقلق إزاء جرعة الإشعاع الفردية ويهتمون على وجه التحديد بمخاطر الإشعاع من التصوير الشعاعي للثدي.

وكان الهدف من هذه الدراسة هو التحقيق في كثافة الإشعاع المستطارة حول أنظمة التصوير الشعاعي للثدي الرقمية الحديثة في ثلاثة مستشفيات في ظل ظروف سريرية. أجريت القراءات باستخدام كاشف الاشعاع العالمي (RADOS 120). تم قياس الإشعة المستطارة على مسافات مختلفة في أربعة مناطق حول وحدة التصوير الشعاعي للثدي. وكانت هذه المناطق هي غرفة التحكم ومكتب التقنيين والمكاتب المجاورة ومنطقة الانتظار لغرفة التصوير الشعاعي للثدي. تم قياس المسافة بين وحدة التصوير الشعاعي للثدي والمناطق الأربعة. وقد اتخذت جميع القياسات في الإسقاط الرأسي الذيلي.

وأظهرت نتائج الدراسة أن قراءات الإشعاع المتناثرة تم الكشف عنها في غرفة التحكم (0.5 ميكروسيفرت/ساعة) والمكتب المجاور (0.2 ميكروسيفرت/ساعة) في المستشفى A. كما تم الكشف عنها في المكتب المجاور (0.9 ميكروسيفرت/ساعة) في المستشفى B، في حين لوحظ في منطقة الانتظار (0.8 ميكروسيفرت/ساعة) في المستشفى C.

ويمكن استخدام قياسات الانتثار هذه في حساب التدريع ومقارنتها بمعايير تصميم التدريع الحالية لتحديد ما إذا كانت هناك حاجة إلى حماية إضافية من الإشعاع أو تغيير في التدريع الحالي

Chapter One
Introduction

1.1 Introduction:

Mammography continues to be the primary imaging tool in the detection of early breast cancer. Because of the overall increase in the use of medical ionizing radiation, many patients and their physicians are appropriately concerned about individual radiation dose and specifically concerned about the risks of radiation from mammography. Although the dose absorbed by the breast and adjacent organs during mammography is a small component of the lifetime accumulated dose from medical imaging and other sources, the popular press tends to emphasize the radiation risk of mammography, particularly screening mammography (Broisman et al., 2011, Ciraj-Bjelac et al., 2010). There is also a lack of knowledge and awareness of radiation doses and safety. Referring physicians, regardless of their area field of practice, underestimate both dose and potential effects (Fartaria et al., 2016).

Physicians are obligated to balance the risks and benefits of various medical procedures while keeping the patient informed of risk-to-benefit ratios. This is particularly important for women of child-bearing age and pregnant women. Knowledge of the scatter radiation dose from screening mammography is important because it enables health care providers to better educate women regarding the radiation risks associated with mammography (Chetlen et al., 2016).

Although direct radiation dose measurements to the breast and predicted radiation-induced breast cancers from mammography have been well documented, doses to other organs from scatter radiation have not been directly measured but have been estimated through computer simulations and the use of phantom models (Svahn et al., 2015).

For all modern mammography units, the primary beam is intercepted by the image receptor assembly. European (Amendoeira et al., 2013) and US (Food and Administration, 2009) guidelines permit only a very narrow strip of the primary beam to overlap the image receptor assembly along the chest wall edge of the beam.

This radiation is usually attenuated to insignificant levels by the patient and, consequently, only secondary radiation must be considered for radiation protection purposes in mammography rooms. Furthermore, it is reasonable to assume that radiation scattered by the patient is the dominant source of secondary radiation, given the minuscule leakage intensity observed at mammography accelerating potentials (Simpkin, 1996).

The aim of this study was to investigate scatter radiation intensity around modern digital mammography systems under clinical conditions. Furthermore, these scatter measurements were substituted into a shielding calculation and results compared with current shielding design criteria to determine whether additional radiation protection or alteration to present shielding was required.

1.2 Problem of the study:

During the use of mammography, dispersal radiation has a risk even if it is a small amount, especially for workers in the department because they are exposed to radiation at all work time.

1.3 Objectives of study:

1.3.1 General Objectives

The general objective of this study was to study the distribution of scattered radiation in a mammography unit during breast radiological examination.

1.3.2 Specific objectives:

The study was carried out to measure scattered radiation in four main areas:

- Control room
- Technician office
- Neighboring office
- Waiting area

1.3.3 Over view of study:

This study consisted of five chapters, with chapter one is an introduction which includes; problem of the study, question study objective and significance of the study. Chapter tow represents comprehensive literature review about different measurement studies, while chapter three is a methodology which include material used to collect the data and method of data acquisition and analysis. Chapter four includes presentation of the result using tables and figures, finally chapter five included discussion, conclusion and recommendation.

Chapter Two

Theoretical Background and Literature Review

2.1 Breast definition:

The breast is the tissue overlying the chest (pectoral) muscles. Women's breasts are made of specialized tissue that produces milk (glandular tissue) as well as fatty tissue. The amount of fat determines the size of the breast. The milk-producing part of the breast is organized into 15 to 20 sections, called lobes. Within each lobe are smaller structures, called lobules, where milk is produced. The milk travels through a network of tiny tubes called ducts. The ducts connect and come together into larger ducts, which eventually exit the skin in the nipple. The dark area of skin surrounding the nipple is called the areola. Connective tissue and ligaments provide support to the breast and give it its shape. Nerves provide sensation to the breast. The breast also contains blood vessels, lymph vessels, and lymph nodes (Zucca-Matthes et al., 2016).

2.2 Breast Anatomy:

A mature female breast has a hemispheric shape and its tissue is composed mainly of variable proportions of glandular and adipose (or fatty) tissue. This distribution is maintained by hormonal influences of menstrual cycles until the menopause, where the glandular tissue decreases and is replaced by adipose tissue. The breast has no muscle and is covered by a thin layer of skin. Furthermore, suspensory ligaments (Cooper's ligaments) are found to support the breast between the skin and the chest wall. In terms of glandular tissue, each breast contains a mammary gland with between 15 to 20 lobes, each of which contains hundreds of tiny lobules where milk is produces when a woman is breast-feeding. During lactation, the breast can increased 3 or 4 times its normal weight and milk flows from the lobules through the lactiferous

ducts and lactiferous sinus ending at the center of the areola, the nipple (Klock et al., 2016).

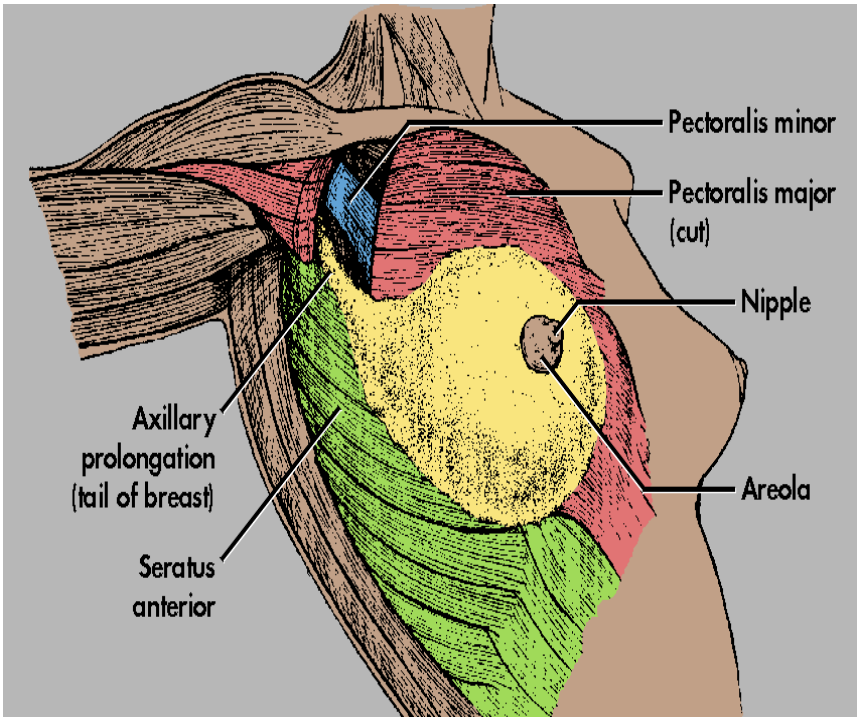

Figure 2.1 Breast anatomy

(https://www.webmd.com/women/picture-of-the-breasts.2014 WebMD, LLC. All rights reserved.)

2.3 Nerve Supply

The breast is innervated by the anterior and lateral cutaneous branches of the 4th to 6th intercostal nerves. These nerves contain both sensory and autonomic nerve fibers (the autonomic fibers regulate smooth muscle and blood vessel tone). It should be noted that the nerves do not control the secretion of milk. This is regulated by the hormone prolactin, which is secreted from the anterior pituitary gland (Vidya and Iqbal, 2017).

2.4 Blood supply of the breast:

The breast receives its blood supply from perforating branches of the internal mammary artery; Lateral branches of the posterior intercostal arteries and several branches from the axillary artery,

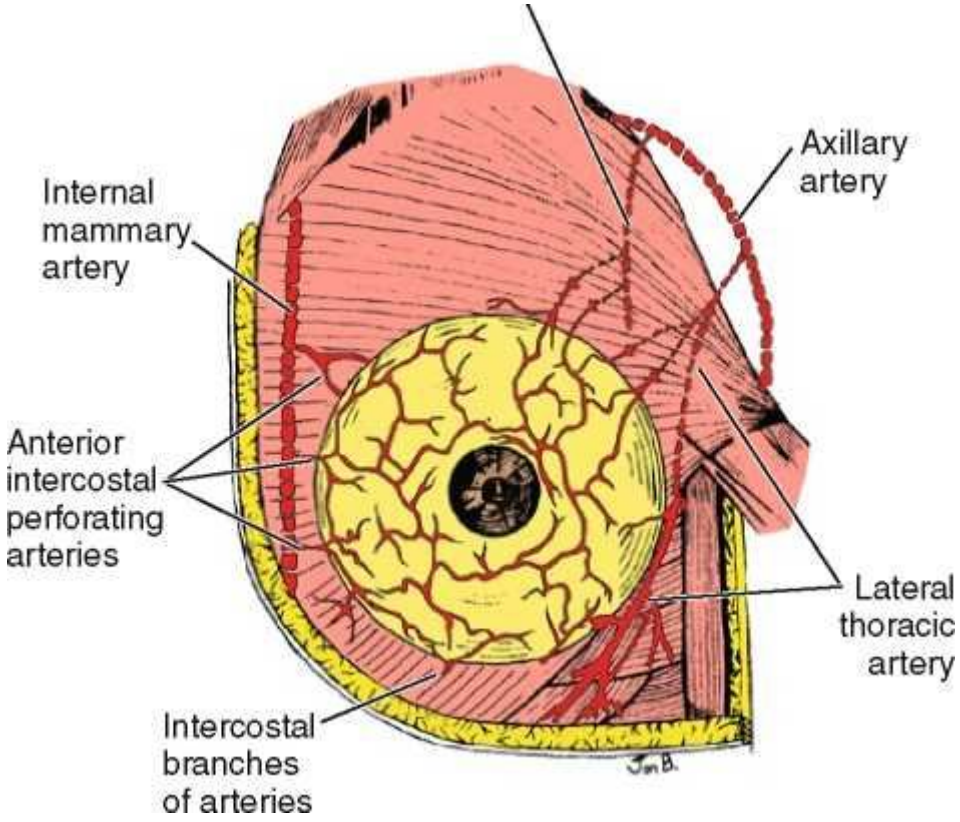

Figure 2-2 Arterial distribution of blood to the breast

(http://aibolita.com/womens-diseases/39967-blood-supply-of-the-breast)

2.5 Breast Cancer:

Internationally, breast cancer has been the cancer of highest incidence and mortality in women. More than 1 million are diagnosed with breast cancer internationally in 2002 with more than 477,000 deaths (Yaffe et al., 2009a). The cause or causes of breast cancer are not completely understood; however, it has been demonstrated that mortality is substantially reduced if disease is detected at

an early stage. Although the probability of developing breast cancer increases with a woman's age (see Table 2.1), the age distribution of the female population causes the percentage of the total breast cancer incidence to vary only slightly with age between the ages 45 and 64 (see Table 2.2). Mammography is an effective method for detecting early-stage breast cancer. It is used both for investigating symptomatic patients (diagnostic mammography) and for screening of asymptomatic women in selected age groups (Hofvind et al., 2017).

In screening, it is the only imaging method that has so far been demonstrated to contribute to reduction of mortality due to breast cancer (Duffy et al., 2005), by the lactiferous duct opening onto the nipple. Within each lobe there are multiple lobules. The terminal ductal lobular unit is the site of origin of most breast disease and is normally only about 3 mm to 5 mm in size. It consists of the extralobular terminal duct and the lobule. The latter is comprised of the intralobular terminal duct and the acini. The arterial supply is primarily from the lateral thoracic and intercostal arteries with branches from the internal mammary artery. The lymphatic system is the route of spread of breast cancer to other parts of the body. The lymphatic vessels drain primarily to the axillary, interpectoral, supraclavicular, and internal mammary nodes. However, there is also free communication to the opposite breast and into the abdomen.

The breast is vestigial in children and men and develops at puberty in women due to stimulation by estrogen and progesterone from the ovaries. However, other hormones such as growth and thyroid hormones, the adrenal corticosteroids, and insulin are also required. The fluctuation in hormone levels during the normal menstrual cycle results in the cyclical proliferation then atrophy of the hormone-sensitive tissues in the breast. This might have an effect on the development of pathological conditions. At menopause, the loss of estrogen and progesterone usually results in a decrease in the amounts of epithelial and connective tissue,

which is observable in the mammogram. However, the common use of hormone-replacement therapy, other endogenous hormones and drugs might actually result in an increase in the parenchymal and stromal tissues at menopause (Eklund et al., 1994).

Table (2.1) Probability of a woman developing breast cancer at different ages

Age group	(Probability of developing breast cancer (%)
40	0.48
40_49	1.43
50_59	2.5
60_69	3.5
70	3.88
Total	12.28

Data from (2005) - (2009)

Table (2.2) Age distribution of female breast cancer incidence (Yaffe et al., 2009b)

Age group	Relative incidence of breast cancer (%)
45	10
45_54	23
55_64	28
65	39
Total	100

Data from (2009)

2.6 Mammography

Mammography is specialized medical imaging that uses a low-dose x-ray system to see inside the breasts. A mammography exam, called a mammogram, aids in the early detection and diagnosis of breast diseases in women. An x-ray (radiograph) is a noninvasive medical test that helps physicians diagnose and treat medical conditions. Imaging with x-rays involves exposing a part of the body to a small dose of ionizing radiation to produce pictures of the inside of the body. X-rays are the oldest and most frequently used form of medical imaging (Timmers et al., 2015).

2.6.1 Digital mammography

Also called full-field digital mammography (FFDM), is a mammography system in which the x-ray film is replaced by electronics that convert x-rays into mammographic pictures of the breast. These systems are similar to those found in digital cameras and their efficiency enables better pictures with a lower radiation dose. These images of the breast are transferred to a computer for review by the radiologist and for long term storage. The patient's experience during a digital mammogram is similar to having a conventional film mammogram (Timmers et al., 2015).

2.6.2 Digital breast tomosynthesis:

DBT is an emerging technology currently under investigation, which could overcome the aforementioned limitations found in 2D planar X-ray mammography. In 2011, the U.S. FDA approved a DBT system (Hologic Selenia Dimensions) to be used clinically; however several other systems are currently being used in Europe (e.g. Siemens Mammomat Inspiration). Clinical results have shown the potential increase in sensitivity when using DBT technology as lesions become clearer to radiologists (Caumo et al., 2017).

DBT geometry differs slightly from manufacturer to manufacturer (e.g. static vs rotating detectors). However, it contains almost all the parts found in FFDM. In fact, some manufacturers integrate DBT technology into FFDM X-ray mammography devices, which is an advantage in economic terms. Unlike FFDM, the X-ray tube is moved in DBT during the acquisition time with respect a rotation point (at or close to the detector) forming an arc as illustrated in Figure 2.3. While the X-ray tube is moved, the X-ray detector can be moved or it can remain static. This produces a series of 2D low-dose X-ray projections of the breast taken at different (but limited) angles, being the total dose similar to the dose observed in FFDM. The raw X-ray projections recorded within the detector for each projection are then processed using a reconstruction algorithm (e.g. filtered back projection), creating a pseudo-3D image representation of the breast. This pseudo-3D image provides cross-sectional views of the breast at different depths, where a given plane (parallel to the detector surface) is shown in sharp focus while the obfuscating anatomical clutter from other planes is displayed out of focus. DBT can achieve very high resolution in the planes parallel to the detector, whereas lower resolution is observed in the planes perpendicular to the detector. However, this resolution is enough to reduce the tissue superposition (Altundag, 2017).

One of the main disadvantages of using DBT is the significantly increased amount of scatter observed in the image receptor for each projection with respect to that encountered in planar X-ray mammography. This is due to the absence of an anti-scatter grid in most of the DBT commercial systems. Generally, the image receptor remains static while the X-ray tube is swept through a limited arc; a conventional fixed anti-scatter grid would absorb much of the primary photons. Thus relatively large scatter fields are present in the projection images which need to be estimated as part of any correction scheme to reduce the contrast-reducing effect of this undesirable component, and to minimize the associated error during reconstruction.

As the tissue superposition problem encountered in FFDM is reduced in DBT, a reduction in the breast compression may be possible. This idea was studied by Saunders et.al. They stated that a breast compression reduction is possible in DBT while maintaining the same imaging performance. Furthermore, this will also mitigate the discomfort of the patient when having the breast compressed during the examination. However, this topic needs further investigation as the compression of the breast has further benefits (Houssami, 2017).

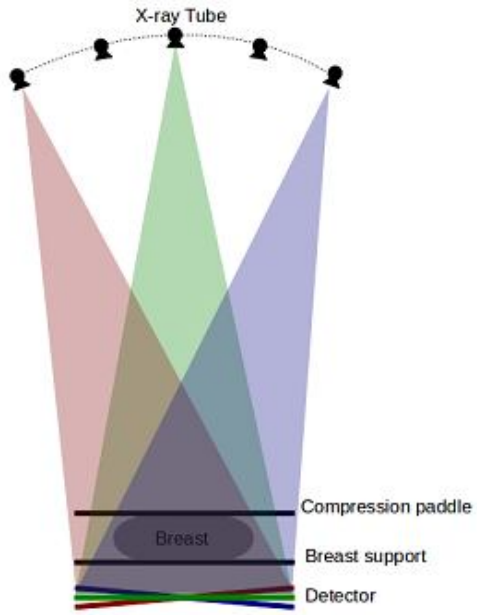

Figure 2.3: Diagram of a DBT system. The breast is imaged at different (But limited) angles.

2.6.3 Mammographic unit:

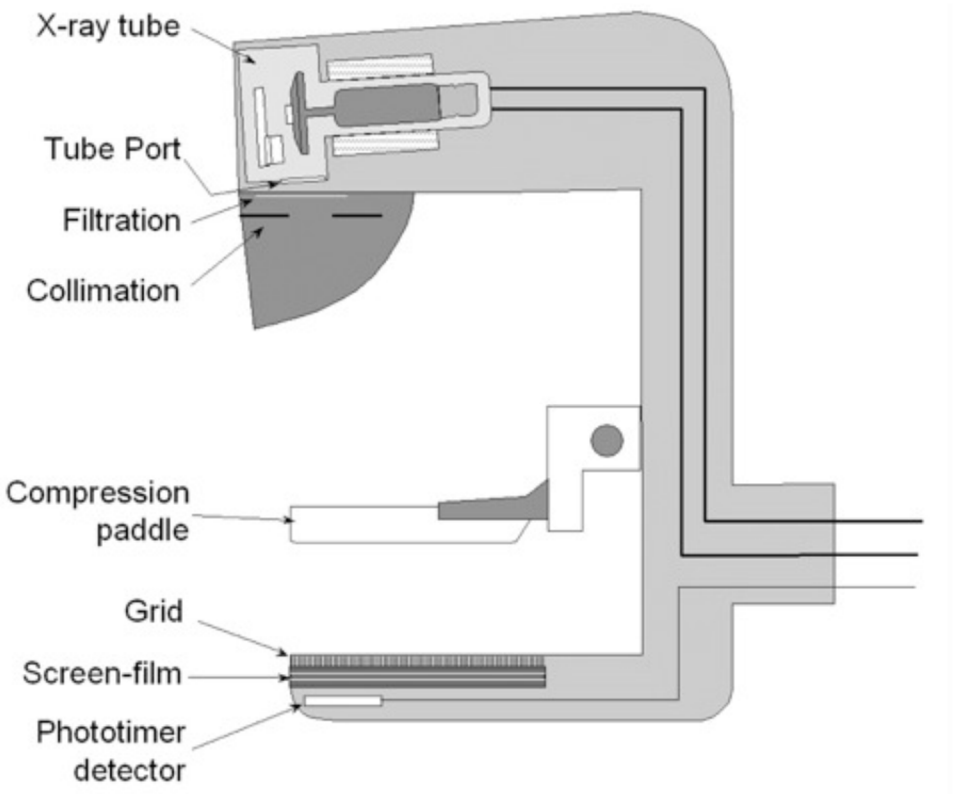

Figure 2.4: Mammographic Unit

(Radiology Physics Lectures: Mammography – 2015)

X ray generator:

- High frequency
- Near constant potential Waveform

X ray tube:

- Rotating anode
- Dual focus 0.3/0.1 mm
- Beryllium exit window (low attenuation)

FID (focus image distance)

generally in the range 60 to 65 cm x-ray spectrum should provide a range of energies that give an appropriate compromise between radiation dose and image quality for the tissues under examination x ray spectrum determined by target material, filter material, and tube voltage (kV) For screen-film mammography optimum beam energy lies between 18 and 23 keV depending on breast thickness and composition (Yaffe et al., 2009a).

Characteristic X rays from molybdenum and rhodium are suitable:

- Higher energies may be more optimal for digital Mammography
- Metallic filters used in mammography
- Molybdenum (Mo) filter (30 to 35 μm thick) commonly employed with Mo anode
- Filter acts as energy window

2.6.3.1 The X-Ray Unit

The components of the imaging system will be described briefly here, while their design will be related to the imaging performance requirements of mammography in later sections. The mammography unit consists of an x-ray tube and an image receptor mounted on opposite sides of a mechanical assembly or gantry. Because the breast must be imaged from different aspects and to accommodate patients of different height, the height of the assembly can be adjusted, most general radiography equipment is designed such that the image field is centered below the x-ray source. In mammography, x-rays for mammographic imaging are produced in a specially designed tube. Electrons emitted by a heated cathode assembly are accelerated in an electric field and focused to strike a positively charged anode. The area on the anode upon which the x rays impinge is referred to as the target or focal spot, and it is made of a material such as molybdenum, rhodium, or tungsten, the choice of which depends on the desired x-ray spectrum. The spectrum consists

of both bremsstrahlung radiation and characteristic x rays specific to the target material (Chevalier del Rio, 2013).

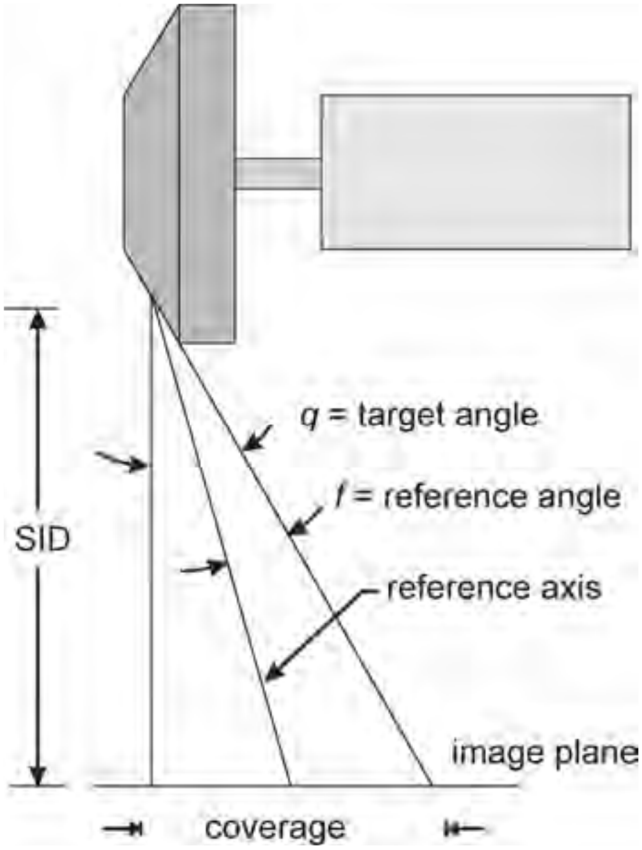

Figure (2.5) Schematic of the anode of a rotating-anode x-ray tube, illustrating the angled surface on which the target material is deposited and the reference axis used for specification of focal-spot size by manufacturers

Both the continuous spectrum of bremsstrahlung photons and the monoenergetic characteristic x-rays are usually referred to in this case as x-rays. In modern mammography systems, a high-frequency (20 kHz) voltage waveform is used to excite x-ray production. This waveform provides an almost constant potential to the tube. Typically, potentials ranging from about 20 kV to 40 kV, chosen according to the thickness and composition of the breast, are applied to the tube for

clinical imaging. Because of the relatively low energy of electrons used in mammography, the efficiency of x-ray production is very low, and most of the kinetic energy of impinging electrons is dissipated in the anode as heat. To accommodate this heat while allowing the effective focal spot size used in image formation to be small, the target is formed on the surface of a rotating anode disk, and the anode is tilted with respect to the incident electrons see Figure (2.5) so that the heat is spread over a greater area. Depending on their angle of emission, x rays formed in the target material must, therefore, traverse different path lengths through the target in traveling from their point of production to the image plane., it is seen that this causes there to be greater attenuation of x rays traveling toward the nipple side of the mammogram than toward the chest wall side. The resultant variation in x-ray influence along the nipple–chest wall axis is referred to as the heel effect. Radiation leaving the x-ray tube passes through a tube port, generally composed of beryllium, a metallic spectrum-shaping filter, a beam-defining aperture, and a plastic plate, that compresses the breast. The compression plate should be reasonably rigid and compress the breast to a uniform thickness, although some manufacturers have employed tilting paddles to improve positioning. Those photons transmitted through the breast and the breast-support platform are incident on an anti-scatter “grid” and then pass through the housing of the image receptor, finally being incident on the image receptor, where they interact and deposit most of their energy locally. Mammography systems are designed to minimize the distance between the breast and the image receptor to keep the magnification factor low and avoid increasing the geometric unsharpness (Chevalier del Rio, 2013).

2.6.3.2 Compression Device

In film-screen mammography, the importance of effective compression cannot be emphasized. Compression causes the breast tissue to be spread out over a larger area and reduced in thickness. This results in a significant reduction in the ratio of scattered to primary radiation1 1 reaching the receptor and an improvement in contrast. Spreading the breast tissue out over a larger area also reduces the superposition of structures, thereby improving the conspicuity of pathology. Because the path length through the breast is reduced, fewer doses is required and exposure time can be decreased. At the same time there is less beam hardening so the radiation has a lower effective energy (better contrast). Finally, with a thinner breast, a lower kVp technique can be selected and, since the breast is more uniform in thickness, a higher contrast film can be employed. Finally, by clamping the breast in place, anatomical motion is reduced. Thus, for a multitude of reasons, firm compression is absolutely essential (Tanner, 1992).

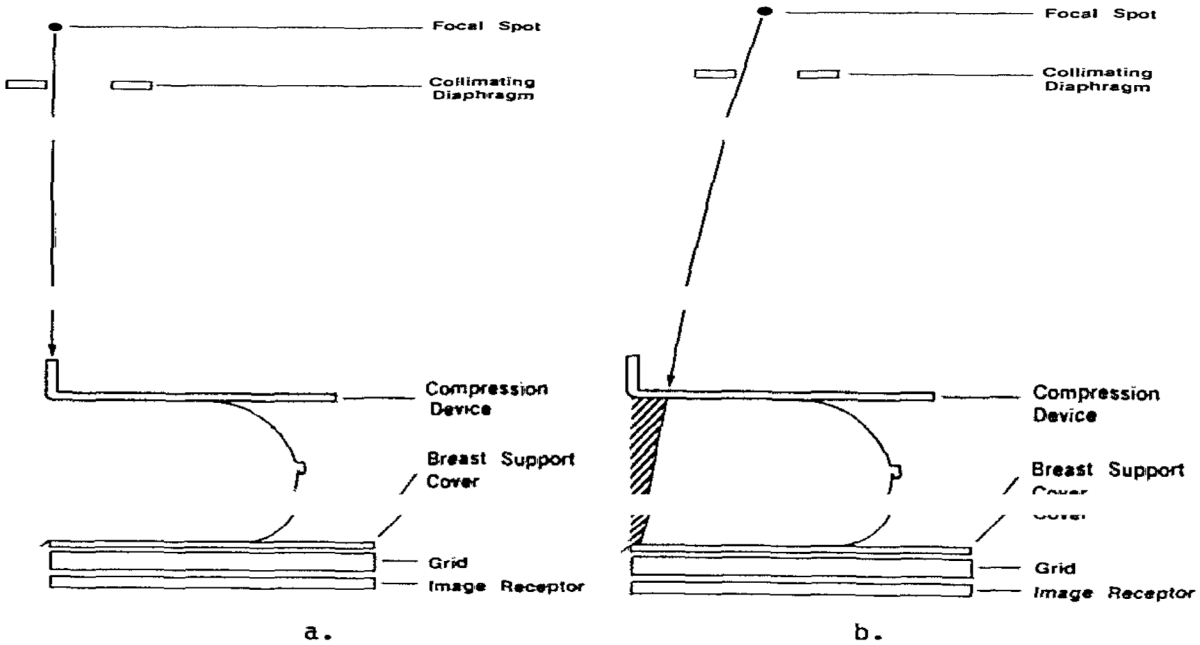

Figure (2.6) X-ray Beam Geometry for Mammography

2.6.3.3 Grid

In mammography of dense or large breasts, image contrast can be reduced markedly by scattered radiation from the breast being recorded by the imaging system. The scatter-to-primary ratio for a breast of average size and density can be 0.6 or greater11. The use of a grid significantly improves image contrast for large or dense breasts. To avoid excessive increase in patient dose, the grid should have a high transmittance of primary radiation. For this reason, carbon-fiber covers and fiber-interspace material are often used. Because of the low energies used in mammography it is important that the covers be of uniform construction so that structural artifacts are not introduced. Typically, a mammographic grid can reduce the scatter-to-primary ratio at the image receptor by a factor of 3 or more while requiring at least a two-fold increase in exposure if the kilovoltage is not raised It has been suggested that a grid will significantly improve the diagnostic quality of mammograms in about 20% of cases12. Where women receive periodic mammography, previous examinations should be used to assess the need for a grid. Reciprocating grids may produce grid lines in cases where the exposure only takes place over a few oscillations of the grid. It is important that the grid assembly be sufficiently rigid that grid motion is not impeded when the breast is under vigorous compression. High strip density (80 lines/cm) aluminum interspace grids that are very thin are also available. These are designed to be placed in or directly above the film-screen cassette and are intended for stationary use. In mammograms produced with stationary grids, grid lines are evident upon close inspection and may interfere with the perception of small, subtle micro calcifications (Napolitano et al., 2002).

High strip density aluminum interspace grids with a grid ratio of 3.5:1 have slightly greater Bucky factors than reciprocating 5:1 fiber interspace grids of lower

strip density. In addition, the aluminum interspace grids do not provide the same degree of contrast improvement. Other practical problems encountered with stationary, high strip density grids are: 1) several grids are needed for efficient patient throughput if they are placed in the film-screen cassettes, 2) they can be easily damaged if they are not mechanically secured to the front of the cassette, and 3) non-uniform grid lines can result in local variations in image density (Perez-Ponce et al., 2013).

2.6.3.4 Focal Spot Considerations

Focal spot nominal sizes of 0.3 to 0.4 mm for contact mammography (breast compressed against the grid and image receptor) and 0.10 to 0.15 mm for magnification imaging (breast compressed against a magnification stand, which supports the breast at a distance from the image receptor to provide geometric image magnification (Mahesh, 2013).

The tube port and added tube filters play an important role in shaping the mammography x-ray energy spectrum. The tube port window is made of beryllium. The low atomic number (Z=4) of beryllium and the small thickness of the window (0.5 to 1 mm) allow the transmission of all but the lowest energy (less than 5 kev) bremsstrahlung x-rays. In addition, Mo and Rh targets produce beneficial K-characteristic x-ray peaks at 17.5 and 19.6 keV (Mo) and 20.2 and 22.7 keV (Rh), whereas tungsten targets produce a large fraction of unwanted L-characteristic x-rays at 8 to 10 keV. Figure 2.7 shows a bremsstrahlung, characteristic and composite x-ray spectrum from an x-ray tube with a Mo target and Be window operated at 30 kV. Added x-ray tube filtration improves the energy distribution of the mammography output spectrum by selectively removing the lowest and highest energy x-rays from the x-ray beam, while largely transmitting desired x-ray energies. This is accomplished by using elements with *K-absorption*

edge energies between 20 and 27 keV. Elements that have these K-shell binding energies include Mo, Rh, and Ag, and each can be shaped into thin, uniform sheets to be used as added x-ray tube filters. At the lowest x-ray energies, the attenuation of added filtration is very high. The attenuation decreases as the x-ray energy increases up to the K-edge of the filter element. For x-ray energies just above this level, photoelectric absorption interactions dramatically increase attenuation as a step or "edge" The result is the selective transmission of x-rays in a narrow band of energies from about 15 keV up to the K-absorption edge of the filter (Mahesh, 2013).

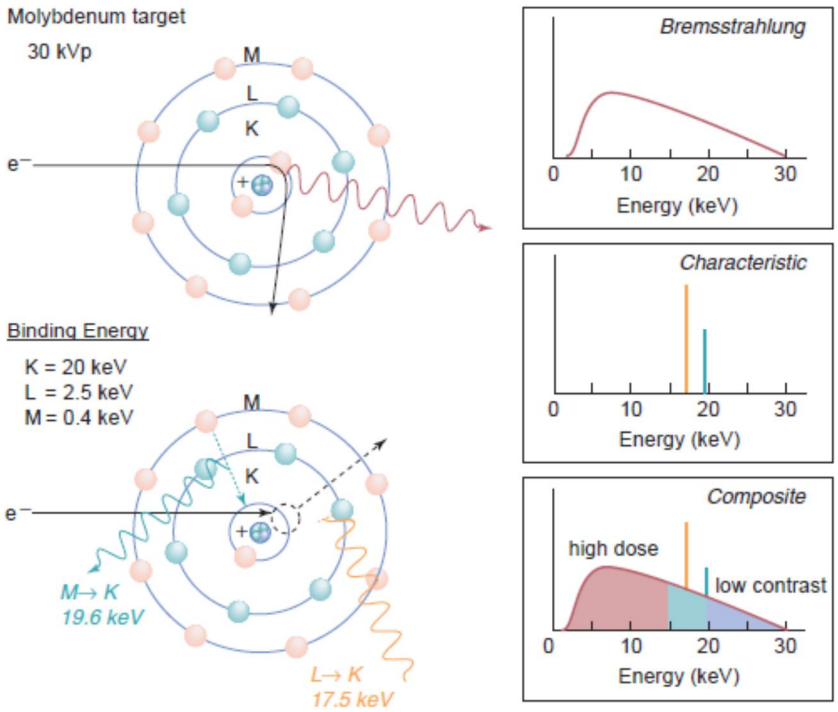

Figure (2.7) the x-ray spectrum of a mammography x-ray tube

The x-ray spectrum of a mammography x-ray tube is composed of bremsstrahlung (with a continuous photon energy spectrum) and characteristic (discrete energies) radiation. A Mo anode tube operated at 30 kV creates the continuous spectrum as well as characteristic radiation with photon energies of 17.5 and 19.6 keV. On the lower right, the "unfiltered" composite spectrum transmitted through 1 mm of Be

(tube port material) has a large fraction of low-energy x-rays that will deposit high dose without contributing to the image, and a substantial fraction of high-energy x-rays that will reduce subject contrast of the breast tissues. The ideal spectral energy range is from about 15 to 25 keV, depending on breast tissue composition and thickness (Mahesh, 2013).

2.6.3.5 Half-Value Layer

The half-value layer (HVL) of a mammography x-ray beam ranges from 0.3 to 0.7-mm Al for the kV range and combinations of target material, filter material, and filter thickness used in mammography (Fig. 8-12). The HVL depends on the target material (Mo, Rh, W), kV, filter material, and filter thickness. Measurement of the HVL is usually performed with the compression paddle in the beam, using 99.9% pure Al sheets of 0.1-mm thickness. A Mo target, 0.03-mm Mo filter, 28 kV, and a 1.5 mm Lexan compression paddle produce a HVL of about 0.35-mm Al, whereas a W target, 0.05-mm Rh filter, and 30 kV produce a HVL of about 0.55-mm Al (Mahesh, 2013).

2.6.3.6 Tube Output and Tube Output Rate

Tube output is a measure of the intensity of the x-ray beam, typically normalized to mAs or to 100 mAs, at a specified distance from the source (focal spot). Common units of tube output are mGy (air kerma)/100 mAs and mR (exposure)/mAs. The kV, target, filter material and thickness, distance from the source, and focal spot size must be specified (Mahesh, 2013).

Table (2.3) REQUIREMENTS FOR MINIMUM HVL IN THE MQSA REGULATIONS (21 CFR PART 1020.30); ACR: WITH COMPRESSION PADDLE

Tube voltage kv	MQSA: kv/100	ACR:kv/100+0.03
24	0.24	0.27
26	0.26	0.29
28	0.28	0.31
30	0.30	0.33
32	0.32	0.35

2.6.3.7 Automatic Exposure-Control

In mammography, the automatic exposure-control (AEC) detector is normally located behind the image receptor. The AEC should be capable of maintaining optical density within ± 0.15 OD as the peak kilovoltage is varied from 25 to 35; and as the breast thickness is varied from 2.5 to 8 cm for each technique - nongrid, grid, and magnification. A range of density selections should be available with each increment increasing or decreasing the film-screen exposure by 15-20%. In addition, there should be adjustments to provide proper compensation for different film-screen combinations. A desirable capability, which would reduce repeats, is for the unit to select the correct AEC mode, focal spot size and mA automatically by sensing the presence of the Bucky assembly or the magnification platform. [Manual override must also then be provided.] Many of the current mammographic units operated in AEC mode have difficulty in yielding images of constant optical density as breast thickness and tube potential are varied. This can be due to several effects: reciprocity law failure of the film for long exposures through large breasts, beam hardening effects on the sensitivity of the sensor, variation in scattered

radiation, sensor offset currents, etc .AEC density setting should be adjusted to bring the film density within the desired range and this setting recorded. An AEC technique chart can thus be developed by repeating this process in a systematic manner provided that a sufficient range of AEC density settings is available. Compensation circuits have been developed15 to maintain approximately constant density over the normal range of breast thicknesses and kilovoltage settings and for the different techniques - nongrid, grid, and magnification. Figure 2.8 compares the density tracking of a modern mammography unit at 28 kVp before and after the installation of such a device. The modification makes the short AEC exposures shorter; leaves the exposure times for average (4-5 cm thick) breasts unchanged, and lengthen the long exposure times. Recently some manufacturers have introduced improvements in their AEC units intended to yield more consistent film densities across varying kVp and breast thickness and densities. These include short pre-exposure "test shots", multi-element sensors, and automatic sensing of compressed breast thickness by means of an encoder on the compression plate (Mahesh, 2013).

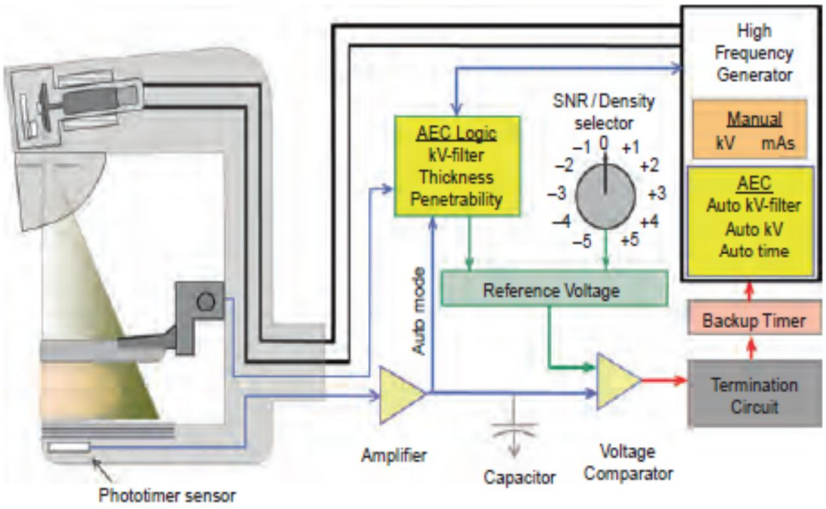

Figure (2.9) automatic exposure control system

2.6.3.8 Scattered Radiation and Antiscatter Grids

X-rays transmitted through the breast contain primary and scattered radiation. Primary radiation carries information regarding the attenuation characteristics of the breast and delivers the maximum possible subject contrast to the detector. Scattered radiation is an additive, gradually varying radiation distribution that degrades subject contrast and adds random noise. If the maximum subject contrast without scatter is C0 and the maximum contrast with scatter is CS, then the contrast degradation factor (CDF) is approximated as

$$CDF=Cs/C0=1/1+SPR$$

where SPR is the scatter-to-primary ratio x-ray scatter increases with increasing breast thickness and breast area, with typical SPR values shown in Figure A breast of 6-cm compressed thickness will have an SPR of approximately 0.6 and a calculated scatter degradation factor of (1/(1+0.6)) = 0.625 = 62.5%. Without some form of scatter rejection, therefore, only a fraction of the inherent subject contrast can be detected. In digital mammography, unlike screen-film mammography, the main adverse effect of scattered x-rays is not a reduction of contrast. Contrast can be improved by any desired amount by post-acquisition processing, such as windowing. The main adverse effect of scatter in digital mammography is that scattered photons add random noise, degrading the signal to noise ratio (Salvagnini et al., 2012).

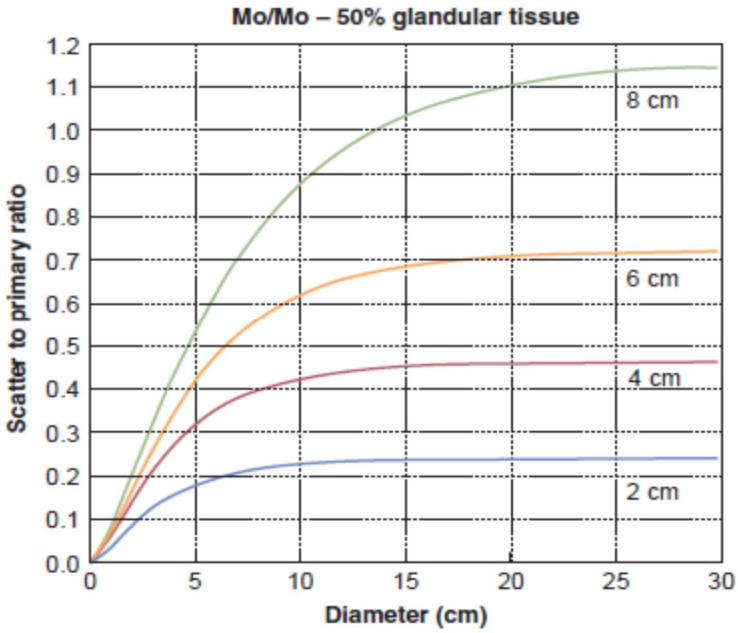

Figure (2.9) scatter radiation ratio

Scatter reduce the radiographic contrast of the breast image. Scatter is chiefly dependent on breast thickness and field area, and largely independent of kV in the mammography energy range (25 to 35 kV). The scatter-to-primary ratio is plotted as a function of the diameter of a semicircular field area aligned to the chest wall edge, for several breast thicknesses of 50% glandular tissue. Scattered radiation reaching the image receptor can be greatly reduced by the use of an *antiscatter grid* or *air gap*. For contact mammography, an antiscatter grid is located between the breast and the detector. Mammography grids transmit about 60% to 70% of primary x-rays and absorb 75% to 85% of the scattered radiation. Linear focused grids with grid ratios (height of the lead septa divided by the interspace distance) of 4:1 to 5:1 are common (e.g., 1.5 mm height, 0.30-mm distance between septa, 0.016-mm septa thickness), with carbon fiber interspace materials (Fig. 2.10 A). Grid frequencies (number of lead septa per cm) of 30/cm to 45/cm are typical. To avoid grid-line artifacts, the grid must oscillate over a distance of approximately 20 lines during the exposure. Excessively short exposures are the cause of most grid-

line artifacts because of insufficient grid motion. A cellular grid, made of thin copper septa, provides scatter rejection in two dimensions (Jing et al., 1998).

Specifications of this design include a septal height of 2.4 mm, 0.64-mm distance between septa (3.8 ratio), a septal thickness of 0.03 mm, and 15 cells/cm. During image acquisition, a specific grid motion is necessary for complete blurring, so specific exposure time increments are necessary and are determined by AEC logic evaluation of the first 100 ms of the exposure. Because of two dimensional scatter rejection and air interspaces, the cellular grid provides a better contrast improvement factor than the linear grid. Grids impose a dose penalty to compensate for loss of primary radiation that would otherwise contribute to SNR in the digital image or for x-ray scatter and primary radiation losses that would otherwise contribute to film optical density in film-screen mammography, the *Bucky factor* is the ratio of exposure with the grid compared to the exposure without the grid to achieve the same film optical density. For mammography grids, the Bucky factor is 2 to 3, so the breast dose is doubled or tripled, but the benefit is improvement of image contrast by up to 40%.

For digital acquisitions, there is no similar “Bucky factor” definition, but the loss of signal in the digital image from primary radiation being attenuated by the grid strips will increase the exposure needed to achieve a similar SNR. Typically, the extra radiation needed for a digital detector is less than the Bucky factor for screen-film, perhaps by one half or more. Grid performance is far from ideal, but digital acquisition and image processing can somewhat mitigate the dose penalty incurred by the use of the antiscatter grid and analog screen-film detectors. An air gap reduces scatter by increasing the distance of the breast from the detector, so that a large fraction of scattered radiation misses the detector (Salvagnini et al., 2012).

The consequences of using an air gap, however, are that the field of view (FOV) is reduced, the magnification of the breast is increased, and the dose to the breast is

increased. However, use of a sufficiently large air gap can render the antiscatter grid unnecessary, thus reducing dose to the breast by approximately the same factor (Jing et al., 1998).

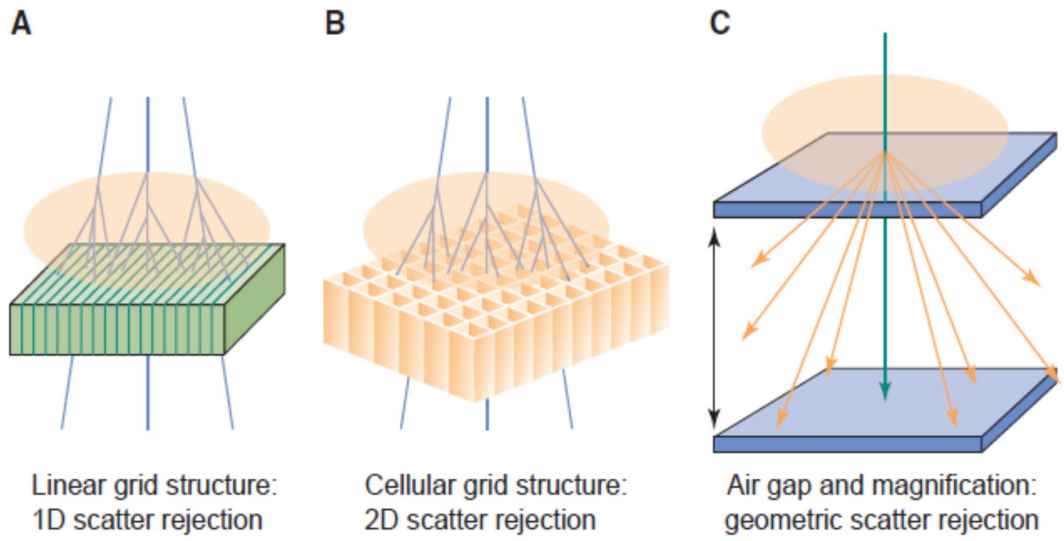

figure (2.10) Antiscatter devices commonly employed in mammography include (A) the linear grid of approximately 5:1 grid ratio and carbon fiber interspace material, (B) a cellular crosshatch grid structure made of copper sheet of approximately 3.8 grid ratio with air interspaces and scatter rejection in two dimensions, and (C) the air gap ntrinsic to the magnification procedure. Note: while the illustration depicts 100% scatter rejection by the grid, approximately 15% of scattered x-rays are transmitted.

2.7 Previous studies

(KEAVEY and PHELAN, 2013) The aim of their study was to investigate the scatter radiation intensity around digital mammography systems and apply these data to standard shielding calculations to reveal whether shielding design of existing breast screening rooms is adequate for the use of digital mammography systems. Three digital mammography systems from GE Healthcare, Hologic and Philips were employed in the study. A breast-equivalent phantom was imaged

under clinical workload conditions and scatter radiation intensities around the digital mammography systems were measured for a range of angles in three planes using an ionization chamber. The results were compared with those from previous studies of film-screen systems. It may be deduced from the results that scattering in the backward direction is significant for all three systems, while scattering in the forward direction can be significant for some planes around the GE and Hologic systems. Measurements at typical clinical settings on each system revealed the Philips system to have markedly lower scatter radiation intensities than the other systems.

(Ducote and S. Molloi, 2010) X-ray scatter is a major cause of nonlinearity in densitometry measurements using digital mammography. Previous scatter correction techniques have primarily used a single scatter point spread function to estimate x-ray scatter. In this study, a new algorithm to correct x-ray scatter based on image convolution was implemented using a spatially variant scatter point spread function which is energy and thickness dependent. The scatter kernel was characterized in terms of its scattering fraction (SF) and scatter radial extent (k) on uniform Lucite phantoms with thickness of 0.8–8.0 cm. The algorithm operates on a pixel-by-pixel basis by grouping pixels of similar thicknesses into a series of mask images that are individually deconvolved using Fourier image analysis with a distinct kernel for each image. The algorithm was evaluated with three Lucite step phantoms and one anthropomorphic breast phantom using a full-field digital mammography system at energies of 24, 28, 31 and 49 kVp. The true primary signal was measured with a multi-hole collimator. The effect on image quality was also evaluated. For all 16 studies, the average mean percentage error in estimating the true primary signal was found to be −2.13% and the average rms percentage error was 2.60%. The image quality was seen to improve at every energy up to

25% at 49 kVp. The results indicate that a technique based on a spatially variant scatter point spread function can accurately estimate x-ray scatter.

Chapter three

Materials and method

3.1 Materials

3.1.1 Machine

This study was carried out in three hospitals in Khartoum state including three mammography machines. The hospital namely; center A, center B and center C.

Table (3.1) shows the feature of the mammography machine (center A):

Specifications	**Machine (A)**	**Machine (B)**	**Machine (C)**
Model	NM-GA	Liyum	Mammomat
Manufactured	Neusoft medical system	Corman (Italy)	SIEMENS
Serial No	G-A-15060003	1 Lil Hf P/ 231/co	55643
Manufactured date	June 18 2015	May 2009	2004
Power supply	220- 250 volt 50/60 Hz	220-240 volt 50/60 Hz	380-480 volt 59/60 Hz
Filtration	0.4 mm	0.5 mm	0.4 mm
Absorption	6.4 kv A	6.6 kv A	5.4 kv A

3.1.2 Survey Meter:

The reading were carried out by using RADOS (RDS-120 Universal Survey Meter, manufacturer: RADOS technology OY Finland, S.No: 20563054 - 990372).

Table 3.2 Specification of RDS-120 Universal Survey Meter

Radiation detected	Gamma and x-rays, 50 keV… 3 MeV. Beta radiation with an external probe
Dose measurement range	0.01 µSv … 10 Sv or 1 µrem...1000 rem
Energy range	50 keV… 3 MeV, within the range of 0.05 µSv/h … 10 mSv/h or 5 µrem/h...1 rem/h 80 keV… 3 MeV, within the range of 10 mSv/h… 10 Sv/h or 1 rem/h...1000 rem/h
Power supply	3 alkaline batteries (IEC LR6), +12 V DC external battery adapter (optional) or AC adapter (optional)

3.2 Method:

For the purpose of this study, the three FFDM systems were operated in manual mode, which allowed selection of kilovoltage, tube current–time product and anode/filter combination. All three systems were subject to routine medical physics quality assurance during the period of this study in accordance with the recommendations of the European Guidelines for Quality Assurance in Breast Cancer Screening and Diagnosis and were found to conform to the standards.

Scatter radiation was measured at different distance in four areas around the mammography unit; these areas were the control room, Technician office, neighboring offices and Waiting area of mammography room. The distance from the mammogram and the four regions was measured. All measurements were taken in Craniocaudal projection

Chapter Four

RESULTS

4.1 Results:

This study was carried out using a RADOS device to measure the scattered radiation around the mammography unit. The distance from the mammography machine and the four areas where it was measured was measured in three hospitals: Center A, Center B and Center C. the following tables show the result of three centers.

Table (4.1) shows exposure factors used

Exposure factors	A	B	C
Kvp	40	35	35
mAs	28	20	18
Projection	CC	CC	CC

The table (4.2) shows scatter radiation measurements in four areas and distance from mammography unit in center A

Location	Scatter radiation (μSv/h)	Distance (cm)
Control room	0.5	100
Technician office	0.0	100
Neighboring offices	0.2	100
Waiting area	0.0	200

The table (4.3) shows scatter radiation measurements in for areas and distance from mammography unit in center B

Location	Scatter radiation (μSv/h)	Distance cm
Control room	0.0	40
Technician office	No	No
Neighboring offices	0.9	50
Waiting area	0.0	100

The table (4.4) shows scatter radiation measurements in four areas and distance from mammography unit in center C

Location	Scatter radiation (μSv/h)	Distance cm
Control room	0.0	30
Technician office	NO	NO
Neighboring offices	0.0	70
Waiting area	0.8	100

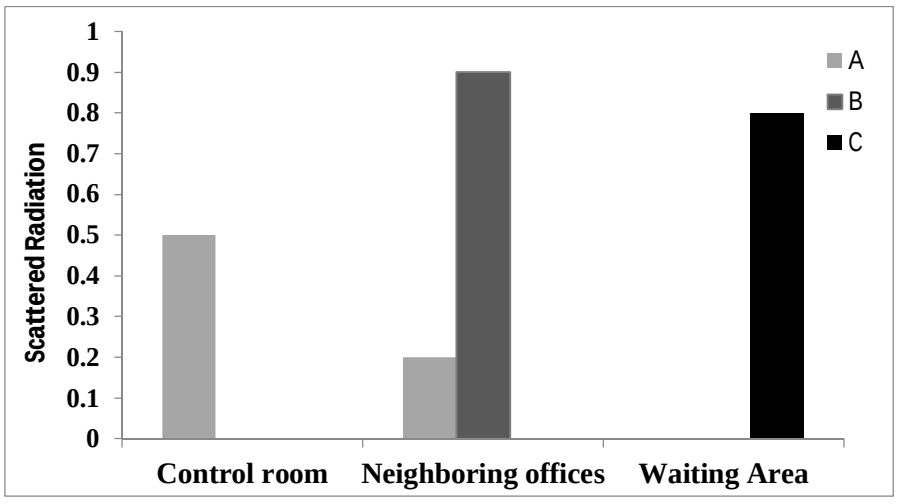

Figure (4.1) comparison of scattered radiation measurements at three centers

Chapter Five

Discussion, Conclusion and Recommendations

5.1 Discussion:

Knowledge of radiation safety during an imaging study is of great interest to radiologic technologist, radiologists, referring physicians, and patients. The magnitude of the risks from low doses of radiation is one of the central questions in radiologic protection and is relevant when discussing the justification for diagnostic medical exposures. This study was carried out using a RADOS device to measure the scattered radiation around the mammography unit in three hospitals.

Regarding center A, the results showed that in control area, scatter radiation is equal to 0.5 µsv/h where the distance between the control area and the mammography unt was 100 cm, in Technician office scatter radiation is equal to 0.0 µsv/h in the distance between the Technician office and the mammography unit was 100 cm, while in Neighboring offices scatter radiation is equal to 0.2 µsv/h where the distance between the Neighboring offices and the mammography unit was 100 cm. Waiting area, scatter radiation is equal to 0.2 µsv/h where the distance between the Waiting area and the mammography unit was 200 cm. Based on the result, it is clearly shown that in center A the scatter radiations levels is in optimal range and the distances were acceptable.

For center B the results showed that in control area, scatter radiation is equal to 0.0 µsv/h where the distance between the control area and the mammography unit was 40 cm, there is no Technician office, in Neighboring offices scatter radiation is equal to 0.9 µsv/h where the distance between the Neighboring offices and the mammography unit was 50 cm. Waiting area scatter radiation is equal to 0.0 µsv/h where the distance between the Waiting area and the mammography device is 100

cm. Based on the result, control area distance was not good and the technician office was not considered in the design, Neighboring offices scatter radiation is about to be high compared to other results, also the waiting area distance was near to the device.

Concerning center C, the results showed that in control area, scatter radiation is equal to 0.0 μsv/h while the distance between the control area and the mammography unit was 30 cm, there is no Technician office, in Neighboring offices scatter radiation is equal to 0.0 μsv/h where the distance between the Neighboring offices and the mammography unit was 70 cm. Waiting area, scatter radiation is equal to 0.8 μsv/h where the distance between the Waiting area and the mammography unit was 100 cm. Based on the result, it was found that control area distance was not good and the technician office was not considered in the design, Neighboring offices scatter radiation is about to be high compared to other results, also the waiting area distance was near to the device.

Finally based on overall results, center A is the best one referring to control area, Technician office, neighboring offices and waiting area.

5.2 Conclusion:

The objective to study the distribution of scattered radiation in a mammography unit during the execution of a breast radiological examination, for the protection of the workers and public. The study compared three centers in terms of scatter radiation which was measured by RADOS and distance which was measured in cm

The study concluded that all centers have readings from scattered radiation which should no be found. However, center A was the best in regarding to control area, Technician office, neighboring offices and waiting area.

5.3 Recommendations:

- Craniocaudal (CC) projection was used in this study; in the futures other projections could be used.
- Mammographic room should follow the design standards.
- Angle of the scattered radiation should be considered.

References:

ALTUNDAG, K. 2017. Digital breast tomosynthesis findings may be different in HER2 positive breast cancer patients according to hormone receptor status. *Br J Radiol***,** 20170730.

AMENDOEIRA, I., ANTTILA, A., BELLOCQ, J., BIANCHI, S., BIELSKA-LASOTA, M., BOECKER, W., BORISCH, B., BOSMANS, H., BROEDERS, M. & RASMUSSEN, B. B. 2013. European guidelines for quality assurance in breast cancer screening and diagnosis.

BROISMAN, A., SCHLESINGER, T. & ALFASSI, Z. B. 2011. Measurement of the radiation dose and assessment of the risk in mammography screening for early detection of cancer of the breast, in Israel. *Radiat Prot Dosimetry,* 143**,** 113-6.

CAUMO, F., ZORZI, M., BRUNELLI, S., ROMANUCCI, G., RELLA, R., CUGOLA, L., BRICOLO, P., FEDATO, C., MONTEMEZZI, S. & HOUSSAMI, N. 2017. Digital Breast Tomosynthesis with Synthesized Two-Dimensional Images versus Full-Field Digital Mammography for Population Screening: Outcomes from the Verona Screening Program. *Radiology***,** 170745.

CHETLEN, A. L., BROWN, K. L., KING, S. H., KASALES, C. J., SCHETTER, S. E., MACK, J. A. & ZHU, J. 2016. JOURNAL CLUB: Scatter Radiation Dose From Digital Screening Mammography Measured in a Representative Patient Population. *AJR Am J Roentgenol,* 206**,** 359-64; quiz 365.

CHEVALIER DEL RIO, M. 2013. [New mammography technologies and their impact on radiation dose]. *Radiologia,* 55 Suppl 2**,** 25-34.

CIRAJ-BJELAC, O., BECIRIC, S., ARANDJIC, D., KOSUTIC, D. & KOVACEVIC, M. 2010. Mammography radiation dose: initial results from Serbia based on mean glandular dose assessment for phantoms and patients. *Radiat Prot Dosimetry,* 140**,** 75-80.

DUFFY, S. W., AGBAJE, O., TABAR, L., VITAK, B., BJURSTAM, N., BJÖRNELD, L., MYLES, J. P. & WARWICK, J. 2005. Overdiagnosis and overtreatment of breast cancer: estimates of overdiagnosis from two trials of mammographic screening for breast cancer. *Breast Cancer Research,* 7**,** 258.

EKLUND, G., CARDENOSA, G. & PARSONS, W. 1994. Assessing adequacy of mammographic image quality. *Radiology,* 190**,** 297-307.

FARTARIA, M. J., REIS, C., PEREIRA, J., PEREIRA, M. F., CARDOSO, J. V., SANTOS, L. M., OLIVEIRA, C., HOLOVEY, V., PASCOAL, A. & ALVES, J. G. 2016. Assessment of the mean glandular dose using LiF:Mg,Ti, LiF:Mg,Cu,P, Li2B4O7:Mn and Li2B4O7:Cu TL detectors in mammography radiation fields. *Phys Med Biol,* 61**,** 6384-99.

FOOD & ADMINISTRATION, D. 2009. Performance standards for ionizing radiation emitting products. *Washington DC: US Government Printing Office,* 21.

HOFVIND, S., SAGSTAD, S., SEBUODEGARD, S., CHEN, Y., ROMAN, M. & LEE, C. I. 2017. Interval Breast Cancer Rates and Histopathologic Tumor Characteristics after False-Positive Findings at Mammography in a Population-based Screening Program. *Radiology,* 162159.

HOUSSAMI, N. 2017. Evidence on Synthesized Two-dimensional Mammography Versus Digital Mammography When Using Tomosynthesis (Three-dimensional Mammography) for Population Breast Cancer Screening. *Clin Breast Cancer*.

JING, Z., HUDA, W. & WALKER, J. K. 1998. Scattered radiation in scanning slot mammography. *Med Phys,* 25**,** 1111-7.

KLOCK, J. C., IUANOW, E., MALIK, B., OBUCHOWSKI, N. A., WISKIN, J. & LENOX, M. 2016. Anatomy-Correlated Breast Imaging and Visual Grading Analysis Using Quantitative Transmission Ultrasound. *Int J Biomed Imaging,* 2016**,** 7570406.

MAHESH, M. 2013. The Essential Physics of Medical Imaging, Third Edition. *Med Phys,* 40.

NAPOLITANO, M. E., TRUEBLOOD, J. H., HERTEL, N. E. & DAVID, G. 2002. Mammographic x-ray unit kilovoltage test tool based on k-edge absorption effect. *Med Phys,* 29**,** 2169-76.

PEREZ-PONCE, H., DAUL, C., WOLF, D. & NOEL, A. 2013. Validation of a digital mammographic unit model for an objective and highly automated clinical image quality assessment. *Med Eng Phys,* 35**,** 1089-96; discussion 1089.

SALVAGNINI, E., BOSMANS, H., STRUELENS, L. & MARSHALL, N. W. 2012. Quantification of scattered radiation in projection mammography: four practical methods compared. *Med Phys,* 39**,** 3167-80.

SIMPKIN, D. J. 1996. Scatter radiation intensities about mammography units. *Health Phys,* 70**,** 238-245.

SVAHN, T. M., HOUSSAMI, N., SECHOPOULOS, I. & MATTSSON, S. 2015. Review of radiation dose estimates in digital breast tomosynthesis relative to those in two-view full-field digital mammography. *Breast,* 24**,** 93-9.

TANNER, R. L. 1992. Mammographic unit compression force: acceptance test and quality control protocols. *Radiology,* 184**,** 45-8.

TIMMERS, J., VOORDE, M. T., ENGEN, R. E., LANDSVELD-VERHOEVEN, C., PIJNAPPEL, R., GREVE, K. D., HEETEN, G. J. & BROEDERS, M. J. 2015. Mammography with and without radiolucent positioning sheets: Comparison of projected breast area, pain experience, radiation dose and technical image quality. *Eur J Radiol,* 84**,** 1903-9.

VIDYA, R. & IQBAL, F. M. 2017. Breast anatomy: Time to classify the subpectoral and prepectoral spaces. *Clin Anat,* 30**,** 434-435.

YAFFE, M. J., BUNCH, P. C., DESPONDS, L., JONG, R. A., NISHIKAWA, R. M., TAPIOVAARA, M. J. & YOUNG, K. C. 2009a. 2. Mammography in Clinical Practice. *Journal of the International Commission on Radiation Units and Measurements,* 9**,** 9-14.

YAFFE, M. J., BUNCH, P. C., DESPONDS, L., JONG, R. A., NISHIKAWA, R. M., TAPIOVAARA, M. J. & YOUNG, K. C. 2009b. Report 82. *Journal of the International Commission on Radiation Units and Measurements,* 9**,** NP-NP.

ZUCCA-MATTHES, G., URBAN, C. & VALLEJO, A. 2016. Anatomy of the nipple and breast ducts. *Gland Surg,* 5**,** 32-6.